

Spatiotemporal persistence of spectral fluxes in two-dimensional weak turbulence

Douglas H. Kelley and Nicholas T. Ouellette

Citation: *Phys. Fluids* **23**, 115101 (2011); doi: 10.1063/1.3657086

View online: <http://dx.doi.org/10.1063/1.3657086>

View Table of Contents: <http://pof.aip.org/resource/1/PHFLE6/v23/i11>

Published by the [American Institute of Physics](#).

Related Articles

Folding dynamics of tethered giant DNA under strong flow
JCP: BioChem. Phys. **5**, 10B614 (2011)

Folding dynamics of tethered giant DNA under strong flow
J. Chem. Phys. **135**, 154901 (2011)

Search for conformal invariance in compressible two-dimensional turbulence
Phys. Fluids **23**, 105101 (2011)

Patterns and dynamics in transitional plane Couette flow
Phys. Fluids **23**, 041301 (2011)

Tracking the dynamics of translation and absolute orientation of a sphere in a turbulent flow
Rev. Sci. Instrum. **82**, 033906 (2011)

Additional information on Phys. Fluids

Journal Homepage: <http://pof.aip.org/>

Journal Information: http://pof.aip.org/about/about_the_journal

Top downloads: http://pof.aip.org/features/most_downloaded

Information for Authors: <http://pof.aip.org/authors>

ADVERTISEMENT

The logo for AIP Advances, featuring the letters 'AIP' in a large, bold, blue font, followed by the word 'Advances' in a smaller, green font. Above the text is a decorative graphic of several orange and yellow circles of varying sizes, arranged in a curved path.

Submit Now

Explore AIP's new
open-access journal

- Article-level metrics now available
- Join the conversation! Rate & comment on articles

Spatiotemporal persistence of spectral fluxes in two-dimensional weak turbulence

Douglas H. Kelley and Nicholas T. Ouellette^{a)}

Department of Mechanical Engineering and Materials Science, Yale University, New Haven, Connecticut 06520, USA

(Received 20 June 2011; accepted 5 October 2011; published online 2 November 2011)

Using a recently developed filtering technique, we study the spatiotemporal properties of the scale-to-scale fluxes of energy and enstrophy in a weakly turbulent experimental quasi-two-dimensional flow. Although these spectral properties vary in time and space, we show that they persist along the Lagrangian trajectories of fluid elements for times that can be nearly as long as the correlation time of the velocity field itself. Additionally, we show that at small scales, the spectral energy flux persists longest for fluid elements in strongly hyperbolic regions of the flow, whereas at large scales it persists in strongly elliptic regions. © 2011 American Institute of Physics. [doi:10.1063/1.3657086]

I. INTRODUCTION

One of the hallmarks of nonlinear systems is coupling and interaction among different length scales. Nonlinearities in real space lead to nonlocalities in Fourier space, which mix contributions from different wavenumbers. In fluid flows, the nonlinear advective term in the Navier–Stokes equations introduces interactions between wavenumber triads that transfer energy and momentum between scales. In three-dimensional turbulent flow, these triad interactions self-organize to drive the classic Richardson–Kolmogorov energy cascade and produce a net spectral flux of energy from large to small scales. In two-dimensional flow, the situation is qualitatively similar but with a key distinction. In two dimensions and in the limit of vanishing viscosity, enstrophy (that is, the square of the vorticity ω , where vorticity is the curl of the velocity) is conserved in addition to energy. This property of two-dimensional flow leads to the Kraichnan–Leith–Batchelor theory of two-dimensional turbulence,^{1–3} which predicts a double-cascade scenario: energy flows via an inverse cascade from the injection scale to *larger* length scales (where it is dissipated by large-scale friction), and enstrophy flows via a direct cascade to smaller scales (where it is dissipated by viscosity). Experimental^{4–7} and numerical^{8,9} studies have long sought to confirm this scenario with measurements of power spectra and the other standard tools of statistical fluid mechanics.

Though power spectra and related quantities do give insight into the spectral transport of energy and enstrophy, recently developed filter-space techniques (FSTs)^{6,10–14} can give much more. Adapted from large-eddy simulation,¹⁵ FSTs allow the direct calculation of the spatiotemporally resolved spectral flux.¹¹ One pioneering study showed that FSTs indicate a double cascade even when fully developed inertial ranges are not apparent in the energy spectrum.⁶ Other work linked the instantaneous spectral transport to the relative orientation of the small-scale stress and large-scale strain-rate tensors^{12,13,16} or to vortices and filaments.¹⁷ These observations were made in the Eulerian framework, in a

coordinate system pinned to the laboratory frame of reference. Significant recent progress in turbulence^{18–20} and scalar mixing^{21–23} has come, however, by focusing on dynamics in the Lagrangian framework and considering individual fluid elements as they move through space and time. As the fluid elements move, they may sample the spatiotemporally varying spectral flux field, which has its own dynamics, non-uniformly. Fluid elements feel the local spectral flux at their position in space and time along their Lagrangian paths, and Eulerian observations alone often give little intuition about the Lagrangian dynamics.

Here, we study the evolution of energy and enstrophy flux along Lagrangian trajectories in experimentally generated quasi-two-dimensional weak turbulence. We calculate spectral-flux fields from experimental measurements using an FST (Refs. 6 and 12–14) and find that, as expected, the spectral properties are smooth in time, space, and scale. We study the Lagrangian dynamics of the spectral flux with autocorrelation functions of the energy (and enstrophy) flux history along the paths of virtual tracer particles. We find that the correlation times for both energy and enstrophy flux are in some cases as long as the correlation time of the velocity field itself, showing that the spectral properties persist for fluid elements. These correlation times, however, vary with length scale in a way that differs strikingly from their Eulerian counterparts and that suggests that advective influences on spectral flux are a function of scale. Measurements of the spatially resolved correlation times indicate that small-scale flux persists longest for fluid elements that explore strongly hyperbolic regions, whereas large-scale flux persists longest for fluid elements in strongly elliptic regions. Our results indicate strong links between spatial transport and spectral flux, and suggest new ways of defining “coherent structures” in turbulent flow that have simultaneously well-defined spatial, temporal, and spectral properties.

II. METHODS

A. Experimental apparatus and flow measurement

We generate quasi-two-dimensional flow in an electromagnetically driven thin-layer apparatus that has been

^{a)}Electronic mail: nicholas.ouellette@yale.edu.

described in detail elsewhere.²⁴ A layer of salt water (4 mm \times 86 cm \times 86 cm, 14% NaCl by mass) lies below a layer of fresh water and above a square lattice of permanent magnets with polarity that alternates in a checkerboard pattern. The lattice length is $L = 2.54$ cm, which sets our energy injection scale. Each magnet is 1.27 cm in diameter and produces a magnetic field of roughly 0.3 T at its surface. Imposing a lateral steady electric current produces Lorentz forces that drive fluid motion. When the forcing is weak, the flow is steady and regular; when the forcing is strong, however, the flow field becomes time-dependent, disordered, and weakly turbulent. We define the Reynolds number of the flow as $\text{Re} = UL/\nu$, where U is the measured root-mean-square velocity and ν is the kinematic viscosity. Here, we show data for $\text{Re} = 185$, above the transition to weak turbulence but in the range where the flow field is still reliably two-dimensional.²⁴

To measure the flow field, we seed the flow with 51 μm fluorescent tracer particles that accurately track the fluid flow. The particles lie on the interface between the saltwater layer and the less-dense freshwater layer. We image the particles with a 4 megapixel digital camera at 60 frames per second, avoiding boundary effects by limiting the field of view to a central 32 cm \times 24 cm region. In the resulting movies we track about 35 000 particles per frame with a multi-frame predictive tracking algorithm;²⁵ particles are typically separated by at least 15 diameters. From the resulting tracks, we calculate Lagrangian particle velocities by convolving the trajectories with a Gaussian smoothing and differentiating kernel.²⁶ Because particles are seeded densely, we can also use them to calculate Eulerian velocity fields. To reduce noise and ensure that the fields are two-dimensional, we project the measured velocities onto a basis of numerically constructed stream function eigenmodes.²⁴

In order to measure Lagrangian statistics, we construct virtual tracer trajectories by numerically solving the equations of motion for fluid elements using the measured velocity fields and a second-order Runge-Kutta integrator.^{27–29} Data from these virtual particles are similar to but smoother than data from actual measured particle tracks, and avoid potential finite-volume biases.³⁰

B. Spatially resolved spectral fluxes

From our measured velocity fields, we obtain energy and enstrophy flux fields with an FST.⁶ The key to this technique is the application of a low-pass spatial filter to the measured fields. Let us define $u_i^{(r)}$ as the i th component of the velocity field filtered at a scale r . The equation of motion for the filtered kinetic energy $E^{(r)} = (1/2)[u^{(r)}]^2$ can then be written as¹¹

$$\frac{\partial E^{(r)}}{\partial t} = -\frac{\partial J_i^{(r)}}{\partial x_i} - \nu \frac{\partial u_i^{(r)}}{\partial x_j} \frac{\partial u_i^{(r)}}{\partial x_j} - \Pi^{(r)}, \quad (1)$$

where summation is implied over repeated indices. The first term on the right-hand side of this equation, as a total divergence, does not modify the total energy in the resolved scales (that is, the scales larger than r), but rather acts as a spatial transport term. The current $J_i^{(r)}$ includes contributions from pressure, advection, and diffusion by molecular and eddy

viscosity.¹¹ The second term is non-positive and represents the direct viscous dissipation of energy at scales larger than r . Since molecular viscosity primarily acts at small scales, this term is typically very small. Both of these terms are analogous with terms that appear in the equation of motion for the full (unfiltered) kinetic energy. The final term, however, is new, and is given by

$$\Pi^{(r)} = -\left[(u_i u_j)^{(r)} - u_i^{(r)} u_j^{(r)} \right] \frac{\partial u_i^{(r)}}{\partial x_j}. \quad (2)$$

In analogy with the new terms that appear after a Reynolds decomposition in the analysis of turbulent flow,³¹ this term can be interpreted as the inner product of the resolved rate of strain and a stress tensor that arises from the coupling between the filtered small scales and the resolved large scales. Since $\Pi^{(r)}$ is not a total divergence, it acts as a source or sink of energy between scales larger than r and those smaller than r , and so its value is a direct measure of the spectral energy flux through the filter scale r . As we have defined it, $\Pi^{(r)} > 0$ denotes transfer to smaller scales (larger wavenumbers), and $\Pi^{(r)} < 0$ denotes transfer to larger scales (smaller wavenumbers). In a similar fashion, we can define a spectral *enstrophy* flux as

$$Z^{(r)} = -\left[(\omega u_i)^{(r)} - u_i^{(r)} \omega^{(r)} \right] \frac{\partial \omega^{(r)}}{\partial x_i}, \quad (3)$$

since the vorticity ω is a scalar in two dimensions.

To implement the FST, we convolve the velocity fields with a spectral low-pass filter. For example, the filtered horizontal velocity is given by

$$u_x^{(r)}(x, y) = \int u_x(x', y') G^{(r)}(x - x', y - y') dx' dy'; \quad (4)$$

other filtered quantities are defined similarly. $G^{(r)}$ is the filter kernel. Following previous work,^{6,11} we use a Gaussian filter; the results for other filter shapes are similar. We exclude a margin at the edge of each flux field to avoid artifacts due to filter ringing at the data boundary, and we do not filter at scales that would exceed the Nyquist limit.

III. RESULTS

Example energy and enstrophy flux fields computed as described above are shown in Fig. 1. As expected, both are smooth in space and exhibit an irregular pattern because of the underlying irregular flow. The flux fields also vary smoothly in time and in scale r . Spatial Fourier transforms of the flux fields confirm that all length scales at least as large as the cutoff scale r are present in each field, as expected. In Fig. 1, we also show the mean (averaged over space and time) energy and enstrophy fluxes as a function of r . Both energy and enstrophy flow away from the injection scale; energy moves primarily toward large scales and enstrophy moves primarily toward small scales, as expected. Both fluxes are strongest near the input scale, and both display some flux in the opposite spectral direction. This oppositely directed flux is stronger for energy, consistent with previous

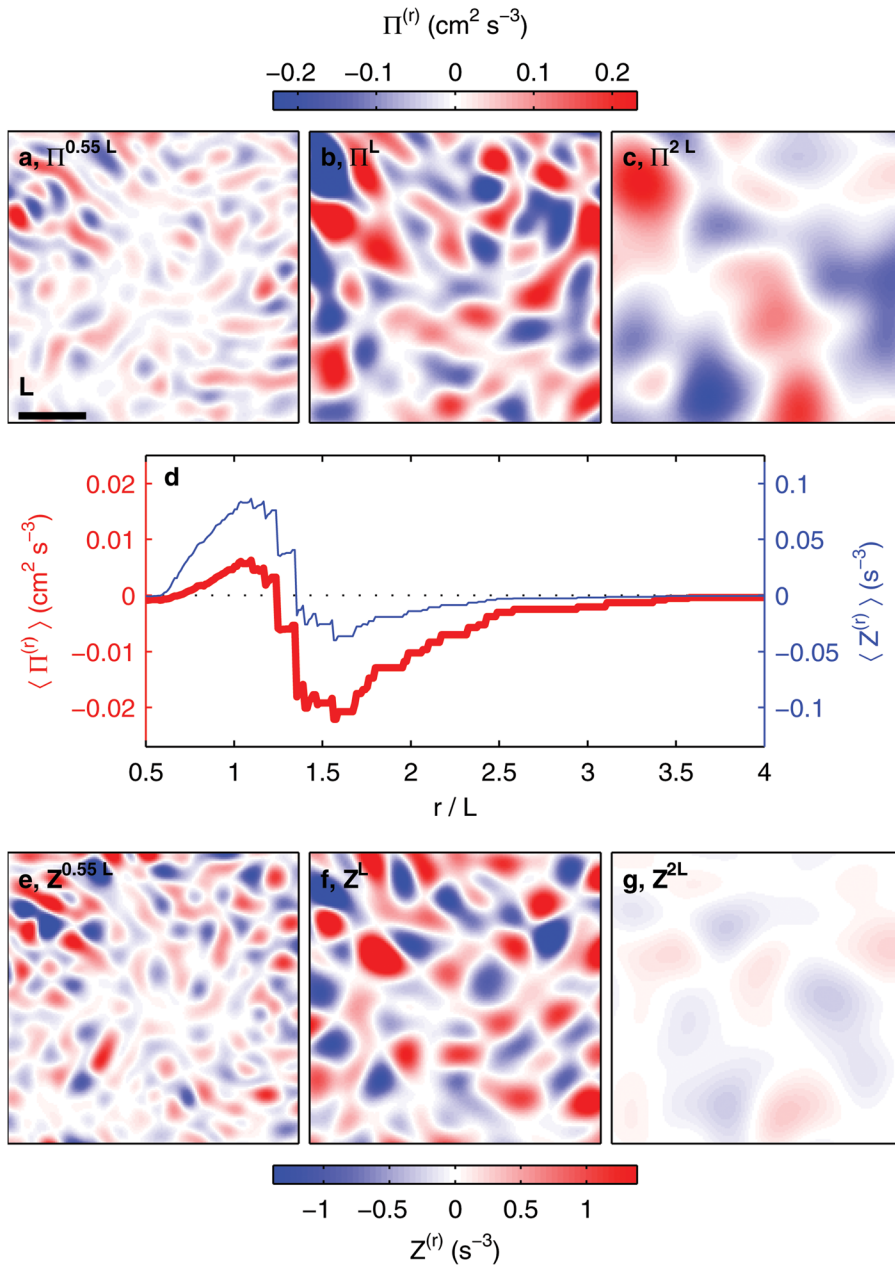


FIG. 1. (Color online) Energy and enstrophy fluxes. (a–c), Spatial variation of energy flux $\Pi^{(r)}$ through scales $r = 0.55L$, L , and $2L$, respectively. Color indicates flux. All panels show the same region and time. (d) Mean energy flux $\langle \Pi^{(r)} \rangle$ (thick line) and enstrophy flux $\langle Z^{(r)} \rangle$ (thin line) as a function of length scale r ; note the differing vertical axes. Energy moves away from L and primarily toward large scales, whereas enstrophy moves away from L and primarily toward small scales. (e–g), Spatial variation of enstrophy flux $Z^{(r)}$ through the same scales as in (a–c).

observations in other systems.^{6,8} The energy and enstrophy cascades can (and do) both act even though energy spectra for our flow do not show well-developed power-law scaling.⁶

The Eulerian fields shown in Fig. 1 are snapshots. But these fields vary in time as well as in space, and so as fluid elements are advected by the flow along their Lagrangian paths, they sample a fluctuating spectral-flux landscape. To understand the Lagrangian nature of the spectral fluxes, we advect virtual tracer particles through the flow fields reconstructed from our experimental measurements^{28,29} and study the spectral fluxes along the resulting trajectories by recording $\Pi^{(r)}$ and $Z^{(r)}$ for different r at each step. Using these Lagrangian histories, we measure the autocorrelation function of the spectral energy flux, defined as³¹

$$\rho_{\Pi^{(r)}\Pi^{(r)}}(s) = \frac{\langle \Pi^{(r)}(t+s)\Pi^{(r)}(t) \rangle}{\langle \Pi^{(r)}(t)^2 \rangle}, \quad (5)$$

where $\langle \cdot \rangle$ denotes an average over the ensemble of Lagrangian trajectories, and the analogously defined autocorrelation function of the spectral enstrophy flux $\rho_{Z^{(r)}Z^{(r)}}$. These autocorrelations are plotted in Fig. 2. As expected, they fall off as a function of time, indicating that the spectral properties decorrelate as the fluid elements evolve. For filter scales smaller than or comparable to the energy injection scale, we observe a brief period of anti-correlation, which we attribute to the close proximity of regions of strong negative and positive flux, as shown in Fig. 1.

In order to quantify the persistence of the spectral fluxes along the Lagrangian trajectories, we also calculate the mean integral timescale, given by³¹

$$\langle \tau_L \rangle = \lim_{T \rightarrow \infty} \int_0^T \rho(s) ds, \quad (6)$$

for each of the various correlation functions $\rho(s)$. These integral timescales are also shown in Fig. 2, normalized by T_L ,

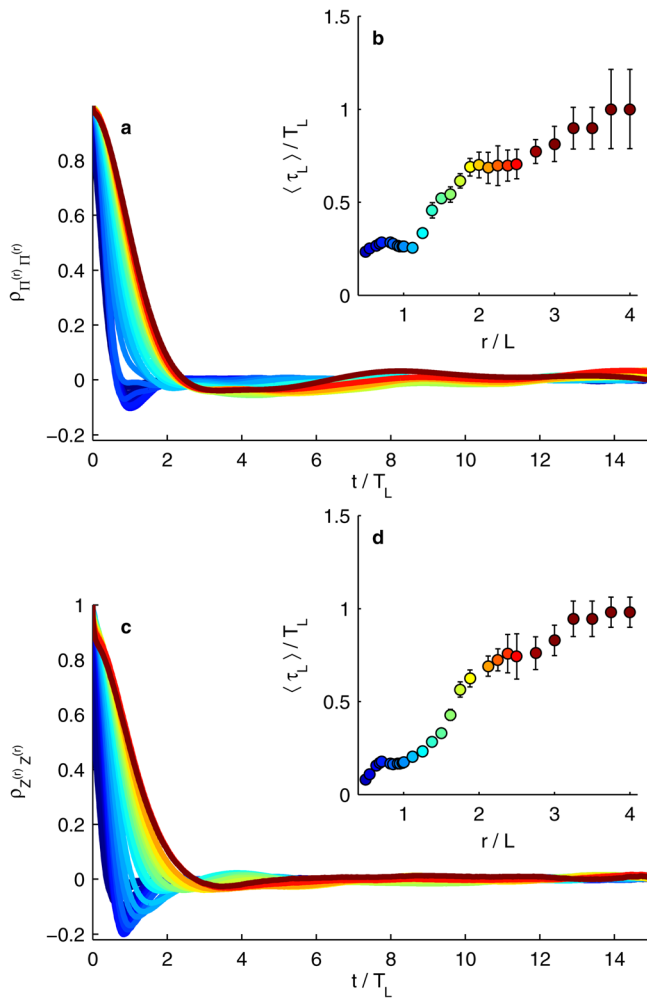


FIG. 2. (Color online) Autocorrelation functions ρ and integral timescales $\langle \tau_L \rangle$ along Lagrangian trajectories for (a,b) spectral energy flux and (c,d) spectral enstrophy flux, for different filter scales r . Times are normalized by T_L , the Lagrangian integral timescale of the velocity field, and lengths by L , the energy injection scale. Correlation functions are plotted in different shades for different scales r ; the corresponding integral timescales are plotted as a function of r . Integral timescales for both energy and enstrophy flux grow rapidly at $r \sim L$, and then slower for $r > 2L$. The error bars show the statistical variation in the mean integral timescales.

the Lagrangian integral timescale of the velocity field. To calculate these integral timescales, we choose values of T (ranging from 2 to $12 T_L$) large enough to capture the shape of $\rho(s)$ but small enough to maintain converged statistics. $\langle \tau_L \rangle$ gives us a measure of how long the spectral-flux properties remain coherent along the trajectories of fluid elements, while T_L tells us how long the velocity field itself remains correlated.³² Surprisingly, the integral timescales of the energy and enstrophy flux vary similarly as a function of r even though their spectral dynamics are very different. For both quantities, the integral timescales at small filter scales ($r < L$) are much smaller than T_L , and are roughly constant. For $L \lesssim r \lesssim 2L$, the integral timescales grow suddenly and rapidly. For larger scales, they grow more slowly (and, for the energy flux at large scales where one might expect an inverse cascade, show a range that is nearly constant), reaching values of $\langle \tau_L \rangle \approx T_L$. Thus, particularly for larger scales, the spectral properties of the flow persist for individual fluid

elements for times that can be as long as the timescale of the flow itself.

The behavior of the temporal *Eulerian* autocorrelation functions (that is, temporal autocorrelations taken at stationary locations) of the spectral fluxes is quite different. In Fig. 3, we show the Eulerian integral timescales of the energy and enstrophy fluxes as a function of filter scale r , normalized by the Eulerian velocity integral timescale T_E . Unsurprisingly, these correlation times show a strong peak at $r = L$, the scale at which energy is injected into the flow. Though it is not fully stationary, the flow at length scales near the injection scale tends to lock onto the forcing lattice, leading to this peak in the correlation time. At other scales, where the flow evolves more dynamically, the spectral properties are correlated for a much shorter fraction of the relevant flow timescale, in sharp contrast to the Lagrangian behavior. The scale-to-scale fluxes thus appear to be more strongly coupled to the *Lagrangian* dynamics of the flow field than they are to the Eulerian dynamics.

To gain further insight into the physics responsible for the differences between the Lagrangian and Eulerian dynamics of spectral transfer, we followed virtual particles along Lagrangian paths in the $\Pi^{(r)}$ field from 5×10^5 initial locations on a regular grid, calculating the integral timescale τ_L of each Lagrangian trajectory individually. We can thus make spatial maps of τ_L , as shown in Fig. 4. (We drop the $\langle \cdot \rangle$ notation to emphasize that these integral timescales are not ensemble averages.) The resulting fields have spatial structure strikingly different from the flux fields shown in Fig. 1, emphasizing the distinction between the Eulerian and Lagrangian dynamics. Mean integral timescales like those plotted in Figs. 2 and 3 are strongly influenced by small regions with very long correlation, given that the tails of the probability density functions (PDFs) of τ_L (also plotted in Fig. 4) are nearly exponential. The regions of long correlation are elongated for $\Pi^{(r)}$ at small scales, as shown in Fig. 4(a). At larger scales, we see larger regions of long correlation with more compact shapes, as shown in Fig. 4(c). At scales r where these larger regions appear, the PDF of τ_L decays more slowly (Fig. 4(d)) and $\langle \tau_L \rangle$ increases (Fig. 2). Thus, a qualitative change in the spatial characteristics accounts for the statistical differences.

This change can be elucidated by comparison with the stretching field of the flow. Stretching, defined as the square

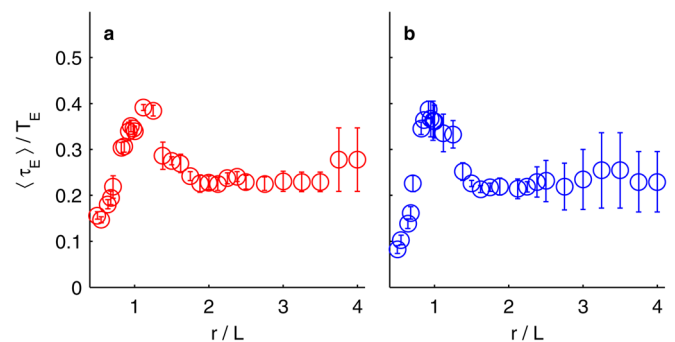


FIG. 3. (Color online) Fixed-point, Eulerian integral timescales $\langle \tau_E \rangle$ of the (a) energy and (b) enstrophy flux, normalized by the single-point Eulerian velocity integral timescale T_E .

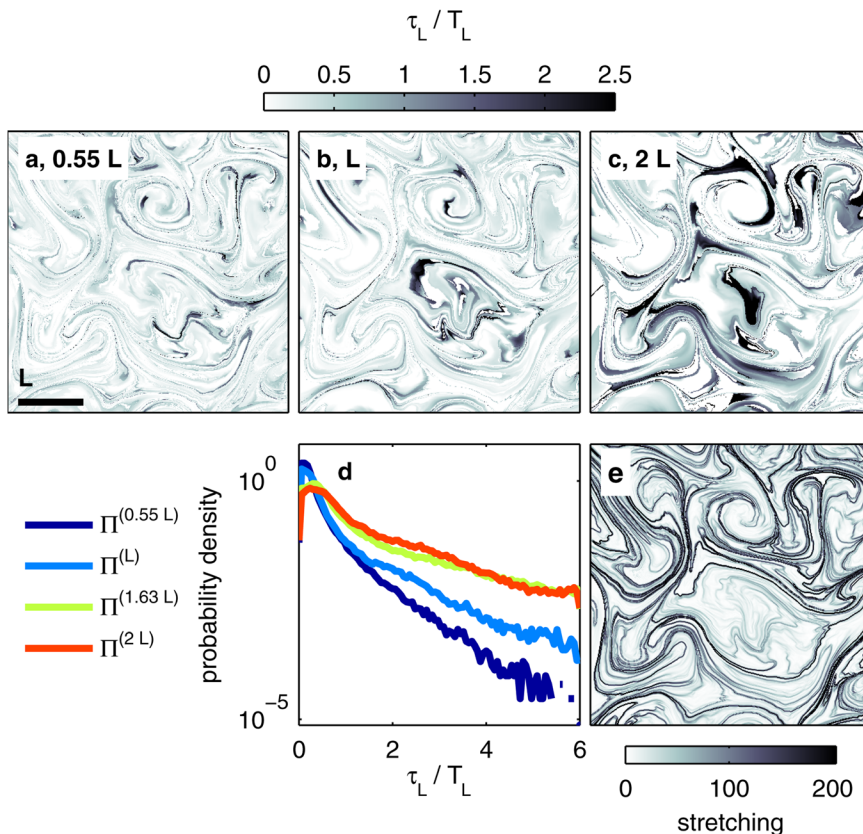


FIG. 4. (Color online) Spatial variation of the Lagrangian persistence of energy flux. (a–c), Integral timescale τ_L of energy flux through scales $r = 0.55L$, L , and $2L$, respectively, in the same region shown in Fig. 1. Shading indicates the local integral timescale, normalized by T_L . (d) Probability density functions of integral timescales τ_L of energy flux through different scales r . For small (large) scales, $\langle \tau_L \rangle$ is dominated by hyperbolic (elliptic) regions. (e) Stretching field in the same region of the flow at the same instant. Darker regions are more hyperbolic.

root of the maximum eigenvalue of the right Cauchy–Green strain tensor,²⁷ is closely related to the finite-time Lyapunov exponents and Lagrangian Coherent Structures.²² Stretching gives a local, Lagrangian measure of hyperbolicity: strong stretching indicates strongly hyperbolic regions, whereas elliptic regions exhibit nearly zero stretching. Eulerian hyperbolicity has previously been associated with strong enstrophy flux.¹² Comparing maps of the integral timescale of $\Pi^{(r)}$ to the stretching field (also in Fig. 4, with integration time $T = 10T_L$), we find that the elongated regions of long correlation that dominate at small scales correspond to regions of strong Lagrangian stretching. Hyperbolicity is coupled not only to strong flux but also to *persistent* flux, especially for scales where an enstrophy cascade is operating. At larger scales, however, the correlation statistics are dominated by regions of long τ_L that correspond not to hyperbolic but rather to elliptic regions of the flow.

IV. DISCUSSION AND CONCLUSIONS

Turbulent fluid flows are characterized by multiscale interactions and spectral cascades. Purely spectral descriptions of the flow, however, neglect the strong spatiotemporal variation of the spectral properties. As we have shown here and as has been demonstrated previously,^{6,12–14,17} the interaction among various length scales is complex, and the energy and enstrophy cascades do not operate uniformly in space. From the viewpoint of a fluid element, what matters is how these spatiotemporally varying spectral fluxes are sampled: how coherent are the spectral dynamics as experienced by fluid elements? In Fig. 2, we showed that,

particularly for fluxes through larger scales in the inverse energy cascade, the spectral dynamics can remain correlated along Lagrangian trajectories for times nearly as long as the fluid velocity field itself. It appears, then, that the spectral dynamics of the flow field persist for fluid elements. When we instead study the correlation time of the spectral flux field at a point, as shown in Fig. 3, we find that the correlation times are shorter relative to the relevant flow timescale, with the spectral fluxes exhibiting some pinning to the forcing structure of the flow. Taken together, these results suggest that the spectral fluxes are at least approximately advected with the flow field in the inverse cascade. The situation is somewhat different in the range of scales in the direct enstrophy cascade; at these smaller scales, the persistence of the spectral fluxes along trajectories is weaker.

It is perhaps surprising that the behavior of the integral timescales for energy and enstrophy are so similar to each other even though the spectral dynamics of these two quantities are so different, as energy is primarily transported upscale and enstrophy is primarily transported downscale. This result suggests that it is not the *magnitude* of the fluxes that determines their spatiotemporal persistence, but rather the *scale*. Further evidence for this effect can be seen in Fig. 5, where we show the integral timescales for the energy flux conditioned on the flux magnitude. The persistence times appear to be independent of the magnitude of the flux. Thus, even though the energy and enstrophy fluxes behave differently as a function of scale, their persistence times along Lagrangian trajectories are very similar.

Much of this effect is likely due to the strong spatial organization of the Lagrangian dynamics of the flow as

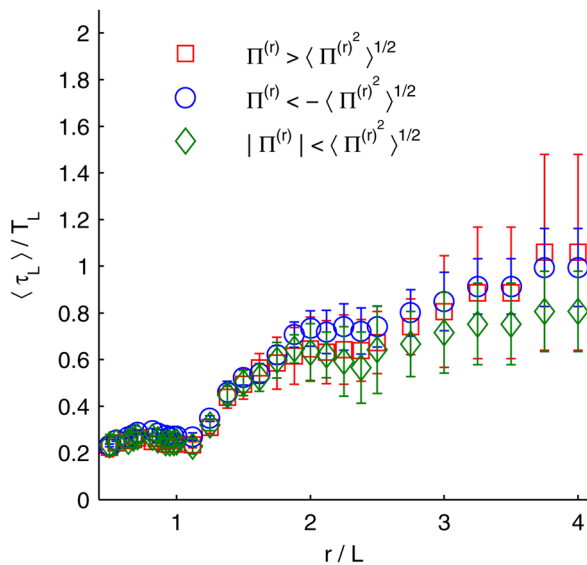


FIG. 5. (Color online) Normalized Lagrangian integral timescales $\langle \tau_L \rangle / T_L$ of the energy flux for correlation functions conditioned on the initial flux magnitude. Data are shown for three cases: $\Pi^{(r)} > \langle \Pi^{(r^2)} \rangle^{1/2}$, $-\langle \Pi^{(r^2)} \rangle^{1/2} < \Pi^{(r)} < \langle \Pi^{(r^2)} \rangle^{1/2}$, and $\Pi^{(r)} < -\langle \Pi^{(r^2)} \rangle^{1/2}$.

revealed by the stretching fields in Fig. 4(e). This “skeleton” of strongly attracting material lines has been shown to have an enormous impact on the transport of fluid elements and scalar fields,^{27,33,34} and so it is not surprising that it plays a similar role here. Both the advection of fluid elements and the spectral fluxes are controlled by the underlying Lagrangian dynamics.

By exploring the Lagrangian structure of the spectral flux in quasi-two-dimensional weak turbulence, we have found that the persistence times of energy and enstrophy are markedly different in the inverse energy cascade as compared to the direct enstrophy cascade. Comparisons with the stretching fields suggest that this difference may be explained in terms of hyperbolic and elliptic regions of the flow. In future work, we hope to develop a quantitative measure of the link between hyperbolicity and persistent spectral flux. These results point to new ways of thinking about dynamical structures in fluid flows as regions that are coherent not only in space and time but also in their spectral properties.

ACKNOWLEDGMENTS

We acknowledge financial support from the U.S. National Science Foundation under Grant No. DMR-0906245.

- ¹R. H. Kraichnan, “Inertial ranges in two-dimensional turbulence,” *Phys. Fluids* **10**, 1417 (1967).
- ²C. E. Leith, “Diffusion approximation for two-dimensional turbulence,” *Phys. Fluids* **11**, 671 (1967).
- ³G. K. Batchelor, “Computation of the energy spectrum in homogeneous two-dimensional turbulence,” *Phys. Fluids* **12**, II-233 (1969).
- ⁴J. Paret and P. Tabeling, “Experimental observation of the two-dimensional inverse energy cascade,” *Phys. Rev. Lett.* **79**, 4162 (1997).
- ⁵M. A. Rutgers, “Forced 2D turbulence: Experimental evidence of simultaneous inverse energy and forward enstrophy cascades,” *Phys. Rev. Lett.* **81**, 2244 (1998).
- ⁶M. K. Rivera, W. B. Daniel, S. Y. Chen, and R. E. Ecke, “Energy and enstrophy transfer in decaying two-dimensional turbulence,” *Phys. Rev. Lett.* **90**, 104502 (2003).

- ⁷H. Xia, H. Punzmann, G. Falkovich, and M. G. Shats, “Turbulence-condensate interactions in two dimensions,” *Phys. Rev. Lett.* **101**, 194504 (2008).
- ⁸G. Boffetta, “Energy and enstrophy fluxes in the double cascade of two-dimensional turbulence,” *J. Fluid Mech.* **589**, 253 (2007).
- ⁹G. Boffetta and S. Musacchio, “Evidence for the double cascade scenario in two-dimensional turbulence,” *Phys. Rev. E* **82**, 016307 (2010).
- ¹⁰M. Germano, “Turbulence: the filtering approach,” *J. Fluid Mech.* **238**, 325 (1992).
- ¹¹G. L. Eyink, “Local energy flux and the refined similarity hypothesis,” *J. Stat. Phys.* **78**, 335 (1995).
- ¹²S. Chen, R. E. Ecke, G. L. Eyink, X. Wang, and Z. Xiao, “Physical mechanism of the two-dimensional enstrophy cascade,” *Phys. Rev. Lett.* **91**, 214501 (2003).
- ¹³S. Chen, R. E. Ecke, G. L. Eyink, M. Rivera, M. Wan, and Z. Xiao, “Physical mechanism of the two-dimensional inverse energy cascade,” *Phys. Rev. Lett.* **96**, 084502 (2006).
- ¹⁴M. Wan, Z. Xiao, C. Meneveau, G. L. Eyink, and S. Chen, “Dissipation-energy flux correlations as evidence for the Lagrangian energy cascade in turbulence,” *Phys. Fluids* **22**, 061702 (2010).
- ¹⁵C. Meneveau and J. Katz, “Scale-invariance and turbulence models for large-eddy simulation,” *Annu. Rev. Fluid Mech.* **32**, 1 (2000).
- ¹⁶Z. Xiao, M. Wan, S. Chen, and G. L. Eyink, “Physical mechanism of the inverse energy cascade of two-dimensional turbulence: A numerical investigation,” *J. Fluid Mech.* **619**, 1 (2009).
- ¹⁷C.-H. Bruneau, P. Fischer, and H. Kellay, “The structures responsible for the inverse energy and forward enstrophy cascades in two-dimensional turbulence,” *EPL* **78**, 34002 (2007).
- ¹⁸G. Falkovich, K. Gawędzki, and M. Vergassola, “Particles and field in fluid turbulence,” *Rev. Mod. Phys.* **73**, 913 (2001).
- ¹⁹A. Arnéodo, R. Benzi, J. Berg, L. Biferale, E. Bodenschatz, A. Busse, E. Calzavarini, B. Castaing, M. Cencini, L. Chevillard, R. T. Fisher, R. Grauer, H. Homann, D. Lamb, A. S. Lanotte, E. Lévêque, B. Lüthi, J. Mann, N. Mordant, W.-C. Müller, S. Ott, N. T. Ouellette, J.-F. Pinton, S. B. Pope, S. G. Roux, F. Toschi, H. Xu, and P. K. Yeung, “Universal intermittent properties of particle trajectories in highly turbulent flows,” *Phys. Rev. Lett.* **100**, 254504 (2008).
- ²⁰F. Toschi and E. Bodenschatz, “Lagrangian properties of particles in turbulence,” *Annu. Rev. Fluid Mech.* **41**, 375 (2009).
- ²¹B. I. Shraiman and E. D. Siggia, “Scalar turbulence,” *Nature (London)* **405**, 639 (2000).
- ²²G. Haller and G. Yuan, “Lagrangian coherent structures and mixing in two-dimensional turbulence,” *Physica D* **147**, 352 (2000).
- ²³D. H. Kelley and N. T. Ouellette, “Separating stretching from folding in fluid mixing,” *Nat. Phys.* **7**, 477 (2011).
- ²⁴D. H. Kelley and N. T. Ouellette, “Onset of three-dimensionality in electromagnetically forced thin-layer flows,” *Phys. Fluids* **23**, 045103 (2011).
- ²⁵N. T. Ouellette, H. Xu, and E. Bodenschatz, “A quantitative study of three-dimensional Lagrangian particle tracking algorithms,” *Exp. Fluids* **40**, 301 (2006).
- ²⁶N. Mordant, A. M. Crawford, and E. Bodenschatz, “Experimental Lagrangian acceleration probability density function measurement,” *Physica D* **193**, 245 (2004).
- ²⁷G. A. Voth, G. Haller, and J. P. Gollub, “Experimental measurements of stretching fields in fluid mixing,” *Phys. Rev. Lett.* **88**, 254501 (2002).
- ²⁸N. T. Ouellette, P. J. J. O’Malley, and J. P. Gollub, “Transport of finite-sized particles in chaotic flow,” *Phys. Rev. Lett.* **101**, 174504 (2008).
- ²⁹S. T. Merrifield, D. H. Kelley, and N. T. Ouellette, “Scale-dependent statistical geometry in two-dimensional flow,” *Phys. Rev. Lett.* **104**, 254501 (2010).
- ³⁰J. Berg, S. Ott, J. Mann, and B. Lüthi, “Experimental investigation of Lagrangian structure functions in turbulence,” *Phys. Rev. E* **80**, 026316 (2009).
- ³¹S. B. Pope, *Turbulent Flows* (Cambridge University Press, Cambridge, England, 2000).
- ³²J. L. Lumley, *Stochastic Tools in Turbulence* (Dover Publications, Inc., Mineola, New York, 2007).
- ³³S. C. Shadden, F. Lekien, and J. E. Marsden, “Definition and properties of Lagrangian coherent structures from finite-time Lyapunov exponents in two-dimensional aperiodic flows,” *Physica D* **212**, 271 (2005).
- ³⁴M. Mathur, G. Haller, T. Peacock, J. E. Ruppert-Felsot, and H. L. Swinney, “Uncovering the Lagrangian skeleton of turbulence,” *Phys. Rev. Lett.* **98**, 144502 (2007).